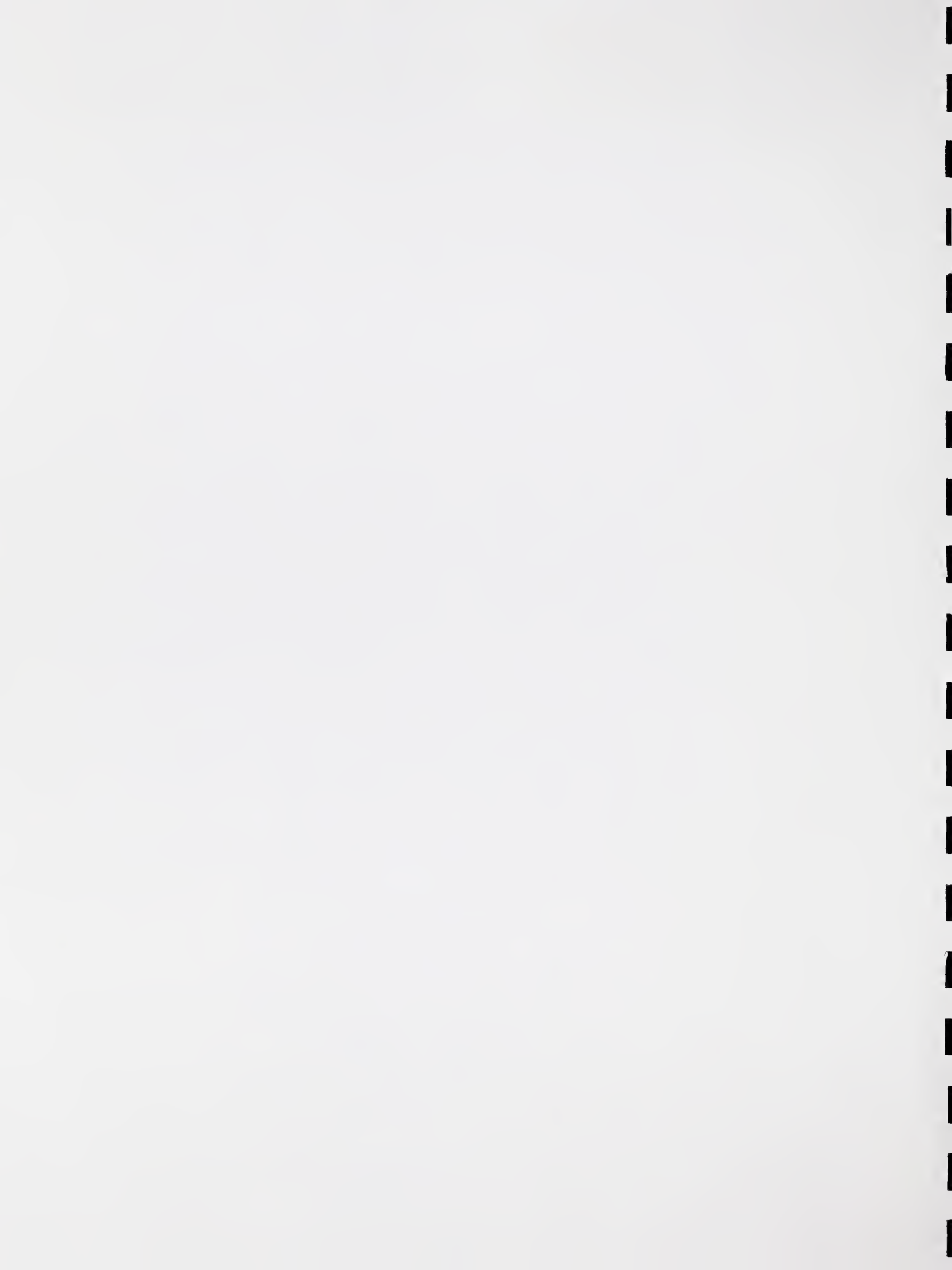# Determination of the Residual Stresses near the Ends of Skip Welds Using Neutron Diffraction and X-Ray Diffraction Procedures

George E. Hicho
Paul C. Brand
Henry J. Prask

U.S. DEPARTMENT OF COMMERCE
Technology Administration
National Institute of Standards
and Technology
Metallurgy and Reactor Radiation Divisions
Materials Science and Engineering Laboratory
Gaithersburg, MD 20899

NIST

Determination of the Residual Stresses near the Ends of Skip Welds Using Neutron Diffraction and X-Ray Diffraction Procedures

George E. Hicho
Paul C. Brand
Henry J. Prask

U.S. DEPARTMENT OF COMMERCE
Technology Administration
National Institute of Standards
and Technology
Metallurgy and Reactor Radiation Divisions
Materials Science and Engineering Laboratory
Gaithersburg, MD 20899

June 1995

Determination of the Residual Stresses near the Ends of Skip Welds Using Neutron Diffraction and X-Ray Diffraction Procedures

By

Paul C. Brand[1], George E. Hicho[2], and Henry J. Prask[3]

Abstract

Welding is known to be a significant factor in the formation of residual stresses. Residual stresses are suspected as the reason for the occurrence of leaks in some railroad tank cars that had stiffeners welded to them. Residual stresses at the surface and in the bulk of metals can be measured non-destructively by x-ray and neutron diffraction respectively. In this report the results of such non-destructive residual stress measurements on one-pass, skip, bead-on plate welds are presented. The plate specimens used for this investigation contained two beads that represent the skip weld process. Of the full weld bead only positions close to the end of the first and the start of the second bead are investigated. The results show longitudinal tensile stresses and compressive transverse and perpendicular residual stresses in the region close to both the weld end and the weld start.

[1]   Paul C. Brand is a guest researcher from the University of Maryland with the NIST Reactor Radiation Division.
Tel. (301) 975 5072.

[2]   George E. Hicho is with the Metallurgy Division, NIST.
Tel. (301) 975 5707.

[3]   Henry J. Prask is with the Reactor Radiation Division, NIST
Tel. (301) 975 6226.

1. Introduction

In 1986, the Federal Railroad Administration (FRA) was informed of the presence of non-conforming welds on a group of several thousand tank cars used to transport hazardous products. The tank cars affected were older cars to which continuous, external axial stiffeners had been added in 1976. The stiffeners ran along the tank car underbelly between the existing stub sills. The purpose of this modification was to increase the tank shell buckling strength to meet an upgraded interchange service specification for compression load (*i.e.*, buff) resistance. Each stiffener was indirectly attached to the tank car shell via a series of narrow rectangular pads. The construction specifications called for continuous fillet welds from the stiffener to the pads, intermittent or "skip" welds from the pads to the tank shell, pad corners and the separation between pads free of weld metal. Figure 1 shows the weld pattern and dimensions for a typical pad. The non-conformance generally involved skip welds which were run together, continued to a pad corner, and/or continued around a corner to fill the pad separation area (see Figure 2). A leak occurred and attention was directed to the pad-to-shell welds. These welds were considered to be possible sources of residual stress which might promote crack formation and subsequent propagation. The FRA Office of Safety requested an assessment of the risk these welds might pose to tank integrity. A theoretical analysis by Orringer *et al.* [1], using finite element and Green's function approaches, revealed for the weld areas in question: "When viewed in the light of the mathematical analysis, it is not surprising that the first crack to have breached one of the reinforced tank cars emanated from a skip weld detail near a broken stiffener ....*etc.*". Experimental work conducted by the Oregon Graduate Institute (OGI) on this same problem, under a grant from FRA, confirmed the general picture of the theoretical analysis and has also stated that these adverse residual stresses are likely to be retained in service [2]. The experimental work was based mainly on the blind hole drilling method [3]. The difficulty of applying this or any destructive evaluation method and the desire to obtain information about the through-thickness distribution of residual stresses led to the present work.

The most widely used non-destructive method to determine residual stresses is x-ray diffraction [4]. In this method, the changes in crystallographic lattice spacing due to the presence of residual stresses are

2

measured. X-ray diffraction, however, is restricted to near surface measurements. Neutrons, on the other hand, because of their much greater penetrating power, can be used for diffraction measurements below the surface in most materials [5]. In order to perform neutron measurements in a timely manner, a high flux neutron source, has to be used. One such source that is available is the NIST Reactor. As an addition to the neutron measurements x-ray diffraction surface residual stress measurements, at selected positions, above where the in-depth neutron diffraction measurements were taken, were also performed.

Understanding the magnitude and distribution of the residual stresses as a result of welding is essential in determining component integrity. Residual stresses arise from non-uniform plastic deformation and can result — as in the present case — from the welding of appurtances to an existing tank car. Welding causes strong local (*i.e.*, non-uniform) plastic deformation, automatically resulting in residual stresses that locally could equal the yield strength of the material. The residual stress field has to be added to the service stress field in order to determine whether crack initiation and propagation may occur within the component. Therefore, depending on their magnitude, direction and location within a component, residual stresses can be either beneficial or detrimental to its performance.

2. Material and welding procedure

Eight steel plates, 61 cm (24 in.) long by 15 cm (6 in.) wide and 1.3 cm (0.5 in.) thick were received from OGI. The plates were reported to be made to ASTM Specification A 515 grade 70 steel. The steel contained these elements, all in weight percent: carbon, 0.31; manganese, 1.20; phosphorus, 0.035 max; sulfur, 0.040 max, silicon, 0.15 to 0.40, and the balance iron. The mechanical properties, according to the ASTM Specification were: tensile strength, 485 to 620 MPa (70-90 ksi), yield strength, 260 MPa, (38 ksi), and a minimum elongation in 50 mm of 21 %.

In Figure 3 a schematic representation of the welding technique applied by OGI is shown. The OGI specimen identification and applied current, travel speed, and leading angle for the plates are summarized in Table 1. In particular, 0.5 cm (3/16 in.) diameter E7018 electrodes were used and the weld type was one pass, skip, bead-on plate. The welding method used

was shielded metal arc (SMAW). The specimens chosen to be examined for residual stresses at NIST were A1, C2, S1, and T2.

3. Measurement Techniques

In this study two techniques for the measurement of residual stresses are employed: neutron diffraction and x-ray diffraction. Both techniques rely on the very precise determination of crystalline lattice spacings and both are based on the same mathematical formalism that ties measured lattice spacings to stresses. The main differences between the two techniques lie in the depth below the specimen surface at which they can be applied and in the way the radiation is produced.

Thermal neutron radiation with a wavelength of about 2.5 Å penetrates about 1000 times deeper into steel than Cr-Kα x-rays, which have a comparable wavelength. In order to reduce the intensity of a neutron beam by a factor 2 it has to pass through 7 mm of iron. The depth — in iron — at which Cr-Kα radiation is reduced to one half of its original intensity is about 5 μm. Using x-rays one can therefore comfortably measure the near-surface stress state of a particular location on a specimen. Unless there is serious evidence of a strong stress gradient (due to grinding for example), this near-surface stress state is usually bi-axial. Neutrons, on the other hand can be used to measure residual stresses in the interior of parts, where the stress state can no longer be assumed to be bi-axial. The fact that at the surface of a specimen the perpendicular component of the stress can be assumed to be equal to zero, makes it possible in the x-ray case to determine the residual surface stress in any direction without having to know the so called stress free lattice parameter. For neutrons, where one has no prior knowledge of the stress state, this is impossible. As a result the x-ray technique has an intrinsic advantage in that one source of potential systematic error is eliminated.

Thermal neutron radiation of sufficient intensity is produced exclusively at laboratories that operate a nuclear reactor and/or a neutron spallation source. X-rays of sufficient intensity can be produced virtually anywhere using a generator and tube arrangement. Neutron diffraction still remains the only absolute technique to nondestructively measure residual stresses below the surface of crystalline materials.

3.1 Theory of Measurement

At this point we will define the specimen axis system to which we will relate the measurements and the stress measurement results. This axis system is given in Figure 4. This study is concerned with residual stresses around the start and stop positions of welds, so our measurement axis system is most readily defined with respect to the orientation of those welds. The direction parallel to the weld is called the longitudinal direction (indicated by "L" in Figure 4). The direction perpendicular to the weld, in the plane of the plate is called the transverse direction ("T" in Figure 4). Finally, the direction perpendicular to the plate is called the normal direction ("Z"). The normal stress components in these three directions are indicated by σ_L, σ_T and σ_Z respectively. Shear components in this axis system are described by τ_{LT}, τ_{LZ} and τ_{TZ} according to the well known Timoshenko definition [6]. These six stress components form a tensor that describes the stress state of a very small volume in a body. Within this axis system, both x-ray and Neutron diffraction can be used to measure crystallographic lattice spacings in a direction that is related to the L, T and Z axes by the so called Eulerian angles φ and ψ as shown in Figure 4. This direction coincides with the direction of the scattering vector **Q**, which is directed along the bisectrix of the incident and diffracted radiation.

The lattice spacing $d(\varphi, \psi)$ is determined by measuring the scattered intensity in a step scan of either the diffraction angle θ or the wavelength of the incident radiation λ. The wavelength or diffraction angle that corresponds to the maximum intensity of the diffraction profile is found by fitting a profile that describes the shape of the diffraction profile. The lattice spacing is then found using Bragg's law for diffraction:

$$2d \; \sin\theta \; = \; \lambda \qquad\qquad (1)$$

If $d(\varphi, \psi)$ is a measured lattice spacing and we assume for a moment that we know the stress free lattice parameter d_0, then the strain $\epsilon(\varphi, \psi)$ in the direction of φ and ψ can be calculated from the relationship:

$$\epsilon(\varphi, \psi) = \frac{d(\varphi, \psi) - d_0}{d_0} \tag{2}$$

From the theory of elasticity we know how these strains can be expressed in terms of the six components of the stress tensor at the measurement site [7]:

$$\epsilon(\varphi, \psi) = \frac{S_2(hkl)}{2}[\sigma_T\cos^2\varphi\sin^2\psi + \sigma_L\sin^2\varphi\sin^2\psi +$$

$$+ \sigma_Z\cos^2\psi + \tau_{TL}\sin2\varphi\sin^2\psi + \tau_{TZ}\cos\varphi\sin2\psi + \tag{3}$$

$$+ \tau_{LZ}\sin\varphi\sin2\psi] + S_1(hkl)[\sigma_T + \sigma_L + \sigma_Z]$$

In equation 3, $S_1(h,k,l)$ and $S_2(h,k,l)/2$ are the so called x-ray diffraction elastic constants. These constants are usually different for different crystallographic lattice planes (h,k,l). They can be obtained from the single crystal values using a polycrystalline model [8] or from calibration experiments [9]. Using neutron diffraction one can measure the lattice strain in six or more different orientations (φ, ψ) and solve the associated set of six (or more) equations with six unknowns. If d_0 enters this set of equations as an extra unknown the set becomes indeterminate, regardless the number of lattice spacing measurements (= number of equations). As a consequence, with neutron diffraction one has to know the stress free lattice parameter d_0 in order to be able to calculate the stresses.

For x-ray diffraction equation 3 is simplified considerably. Because at a free surface no tractions act, both the stress normal to the surface (σ_Z) and shears acting in the plane of the surface (τ_{LZ} and τ_{TZ}) have to be equal to zero so that equation 3 can be simplified to:

$$\epsilon(\varphi, \psi) = \frac{S_2(hkl)}{2}[\sigma_T\cos^2\varphi\sin^2\psi + \sigma_L\sin^2\varphi\sin^2\psi +$$

$$+ \tau_{TL}\sin2\varphi\sin^2\psi] + S_1(hkl)[\sigma_T + \sigma_L] \tag{4}$$

Differentiation of equation 4 with respect to $\sin^2\psi$ and using equation 2 yields:

6

$$\frac{\partial d(\varphi, \psi)}{\partial (\sin^2 \psi)} = d_0 \frac{S_2(hkl)}{2} [\sigma_T \cos^2 \varphi + \sigma_L \sin^2 \varphi + \tau_{TL} \sin 2 \varphi] \qquad (5)$$

In equation 5 d_0 appears as a factor only and can therefore with marginal loss of accuracy be replaced by a d-value associated with some direction (φ, ψ). Equation 4 can be used to obtain values for σ_L, σ_T and τ_{LT} by determining the partial derivative (*i.e.*, the slope of a curve of $d(\varphi, \psi)$ *vs.* $\sin^2 \psi$) for three different values of φ and solving the resulting set of three equations with three unknowns.

3.2 Measurement Procedures

3.2.1 NEUTRON DIFFRACTION

Each specimen is placed on top of a two axis translator which is mounted on the specimen holder of a two axis rotation device (Eulerian cradle), which in turn is mounted on the specimen table of a triple axis neutron spectrometer, which is operating in a double axis mode. Both horizontal translation directions and both angular orientations are automated. Vertical translation can be achieved by hand. Neutron absorbing apertures in the incident and diffracted beams reduce the size of the gauge volume to a cube of $3 \times 3 \times 3$ mm^3. Using a series of alignment procedures that has been described in detail elsewhere [10], the gauge volume was centered on the spectrometer axis and the surface position of the specimen was tied to the instrument axis system. As a result the position of the gauge volume within the specimen is known to better than 0.1 mm in all three directions. The BCC α-iron (110) lattice spacings were then determined using a technique called a wavelength scan. In this technique, the wavelength of the incident neutron radiation is varied in small increments, while keeping the neutron detector at a fixed scattering angle of 2θ equal to 90° (thus the diffraction angle ν equals 45°). Finally the resulting diffraction peak is fitted with a function which itself is the sum of a Gaussian and a Lorentzian function. One of the fit results is the wavelength at which the maximum intensity occurs. From this the Fe (110) lattice spacing is calculated according to equation 1. For each plate the process is repeated at the five different orientations (φ, ψ) given in Table 2. Measurements were performed at 54 positions as indicated in Figure 5.

The stress free lattice spacing d_0 was obtained from a separate set of measurements taken from an as received unwelded plate made of the same steel as the welded specimens. It was verified that d_0 did not change significantly with orientation and position in that plate. At positions in the weld and in the heat affected zone around the weld, d_0 is known to change somewhat as a result of the redistribution of alloying elements (in particular carbon) associated with the metallurgical processes that take place during welding [11]. The effect of d_0-changes on the stress measured by means of neutron diffraction can be significant, so values taken from places that are within the heat affected zone (most likely only those positions at the cross of the "T" in Figure 5) have to be treated with some caution.

Considering the set of measurement orientation angles from Table 2 in relation to equation 3 it is seen that one can solve for σ_L, σ_T, σ_Z and τ_{LT} exactly, while the two other shears: τ_{LZ} and τ_{TZ}, remain unknown. These shears remain unknown because their coefficients in equation 3 ($\cos\varphi\sin2\psi$ and $\sin\varphi\sin2\psi$ respectively) are always equal to zero for this particular set of orientations. Equally true is that the presence of these two unknown shears has no effect on the values of the stresses that one can solve for.

3.2.2 X-RAY DIFFRACTION

After the neutron diffraction stress measurements were finished, the plates were sent to Lambda Research in Cincinnati, OH for surface residual stress measurements using x-ray diffraction. These measurements were performed at three positions at the stop and start positions of each weld as indicated in Figure 5. Prior to measurement, the surface of the plate was cleaned and the upper 0.25 mm of metal was removed by means of electropolishing.

The method used to determine the surface stresses is a two angle $\sin^2\psi$ technique in accordance with GE specification 4013195-991 and SAE J784a. For this application we employed the diffraction of Cr-Kα radiation from the (211) planes of the BCC structure of α-iron. The irradiated surface area was a square spot of 2.5×2.5 mm^2. It was verified separately by measuring the lattice spacing d at six values of $\sin^2\psi$ (0, 0.1, 0.2, 0.3, 0.4 and 0.5), that the d vs. $\sin^2\psi$ curve was sufficiently straight to

rely on just two lattice spacing measurements to determine its slope. The two chosen orientations were $\psi = 10°$ and $\psi = 50°$.

Slope measurements (*i.e.* determining d at two values of ψ) were performed at three values of φ: 0°,45° and 90°. Eventually equation 5 was used to solve for σ_L, σ_T and τ_{LT}.

4. Results

In Figures 6 to 9, the neutron residual stress measurement results: σ_L, σ_T, σ_Z and τ_{LT}, as well the x-ray residual stress measurement results: σ_L, σ_T and τ_{LT} are presented for specimens A1, C2, S1 and T2. Cross references to the numerical values belonging to these figures are tabulated in Tables 3 to 6. It is again noted here that no separate measurement of the stress free lattice parameter has taken place. Neutron measurement results from the point at the "T"-cross at 3 mm depth should therefore be treated with some caution. These values may be affected by a d_0 change due to the fact that this point is at least partly situated in the heat affected zone. The x-ray values close to the weld are not affected by any changes in d_0 and are therefore in principle rigorous.

5. Discussion

A complete stress state of a point in a specimen can be presented in many ways. One way is to give the six individual elements of the stress tensor at that point, relative to a user defined axis system. This is the option chosen here. Another way is to give the three values for the principle stresses and the direction that they act relative to the user defined axis system. The principle stress directions are defined as the three orthogonal directions in which the shear stresses vanish. Since we have no information about the values of τ_{LZ} and τ_{TZ}, we cannot give the complete principle stress information. What can still be done, however, is interpret the one shear value that has been measured: τ_{TL} as a measure of how far the principle axis system is rotated with respect to the chosen specimen axis system around the Z direction. From the results of the shear stress measurements τ_{TL} it is clear that the principle stress axis system rotates around the Z direction with increasing transverse (T) distance from both

9

weld tip positions. The fact that τ_{TL} has opposite signs on opposite sides of the weld is compatible with the fact that due to the weld symmetry the principle axis system must rotate in opposite directions at opposite sides of the weld.

The surface x-ray measurements for σ_L, σ_T and τ_{LT} are consistent with the sub-surface neutron values with the exception of one entire tip location in specimen S1. Unlike in the other specimens, the longitudinal stress at the end of the weld measured using the two techniques do not match. At this point one should realize that the x-ray and neutron measurements closest to the surface are taken at positions which still are an average of 2 mm apart in depth. Also, the neutron measurements average over a much larger depth than the x-ray measurements. The x-ray measurements are therefore much more likely to pick up a local surface distortion in the material (such as a dent by a hammer used to remove slag after welding). The x-ray measurement could be repeated at a somewhat larger depth (*i.e.* by further etching) at which time we expect better agreement between x-ray and neutron measurements on specimen S2.

At the weld start on specimen C2, unlike at all other positions, the neutron σ_Z-values were found to be close to zero. We have no explanation for this other than it being related to the way the weld was fabricated *i.e.* the welding parameters.

The observed transverse stresses σ_T on the other hand, are highly compressive with no significant change with depth below the surface (Z). They decrease with distance from the weld in the transverse (T) direction and the data suggest an increase with longitudinal (L) distance from the weld tips. This suggests an absolute minimum somewhere halfway between the weld tips. These stresses must be balanced by tensile values at the same distance from the weld but at positions half way along each weld bead, as has been reported elsewhere [12]. The existence of high transverse residual stresses at points halfway along the weld bead can easily be verified by measurements there. It has to be realized that these plates were not constrained during welding. As was pointed out by Masubuchi [13], a constraint lateral to the weld adds a (tensile) reaction stress to the transverse stress. The skip welds as part of a real tank car are certainly under more lateral constraint than those in the current sample

plates. The tangential stress level reported here is therefore almost certainly an underestimate.

In our analysis, we found the longitudinal stresses σ_L to be tensile and highest close to the surface at positions close to the weld tip positions (see Figures 6a, 7a, 8a and 9a). At their maximum, the observed stress values are as high as or even higher than the reported yield strength of the steel, 260 MPa (38 ksi). The longitudinal stress diminishes in all three investigated directions: L, Z and T. The result is a small but intense longitudinal tensile stress field directly around the weld tips. This does not mean that the residual stresses are maximum at the weld tip, they could well be even larger along the weld bead itself. There, however, no measurements were taken. According again to Masubuchi [13], mechanical constraints have little or no effect on the longitudinal residual stress level.

The longitudinal direction is the same direction as in which the additional loading occurs during the use of the tank cars, both through the pay-load per car (bending of tank) and the fact that the car is part of the consist (draft and buff). These longitudinal stresses could possibly enhance the probability of crack formation, through a variety of mechanisms of which we consider fatigue the most prominent. Because of the high longitudinal stresses close to the weld tip, we theorize that the initial direction of crack propagation should be perpendicular to the weld direction. In principle and due primarily to the presence of the high longitudinal tensile stresses, crack initiation can take place anywhere along the weld bead region. With subsequent crack growth the longitudinal stresses are relaxed and the crack might enter a region where the transverse stress is high in tension (see above). This could force the propagated crack to turn 90° and continue propagating parallel to the weld direction through the region of high tensile transverse stress. This mode of crack propagation has been observed in the field. This theory is somewhat speculative, because it is based primarily on the assumption that the measured compressive stresses are balanced by tensile stresses alongside the weld bead in the test specimen. As pointed out above, however, the lateral constraints on the skip welds on a real tank car can only lead to increased transverse stress levels. Thus far no attempt has been made to measure them. Proving the existence of such transverse tensile stresses is highly important and should be considered.

6. Conclusions

At and around both start and end positions in a skip, bead on plate weld pair, high tensile residual stresses develop in the direction longitudinal to the weld. These stresses, when added to a longitudinal service load could help initiate a crack and stimulate crack growth perpendicular to the weld bead.

Compressive transverse residual stresses in the vicinity of the skip weld bead extremes, predict the presence of tensile transverse stresses at locations along the weld bead itself. These transverse tensile stresses could take over the crack propagation process once a crack tip enters such locations.

Acknowledgement

References

1. O. Orringer; J.E. Gordon; Y.H. Tang and A.B. Perlman, *Applied Mechanics Rail Transportation Symposium 1988*, AMD-Vol. 96/ RTD-Vol. 2., H.H. Bau; T. Herbert and M.M. Yavanovich, Book No. G00456, pp 87-94, (1988).

2. W.Y. Shen, P. Clayton, and M. Scholl. "Residual stress measurement at skip fillet welds", *Proceedings Practical Application of Residual Stress Technology*, Edited by Clayton Ruud, Indianapolis, IN, 15-17 May 1991.

3. See for example: ASTM E 837-92, *Standard Test Method for Determining Residual Stresses by the Hole-Drilling Strain Gauge Method.*

4. M.E. Hilley, J.A. Larson, C.F. Jatczak, and R.E. Ricklefs, *Residual Stress Measurements by X-ray Diffraction, SAE Information Report J784a*, SAE Inc., Warrendale, PA (1971).

5. A.J. Allen; M.T. Hutchings and C.G. Windsor, *Adv. Phys.*, **34**, 445 (1985).

6. S. Timoshenko and J.N. Goodier, *Theory of Elasticity*, McGraw-Hill Book Company, p3-10, (1951).

7. See, *e.g.*, H.J. Prask and C.S. Choi, *J. Nucl. Mat.* **126**, pp 124-131 (1984) and references cited therein.

8. A. Reuss, *Z. Angew. Math. Mech.* **9**, 49-58 (1929).

9. P.C. Brand; R.B. Helmholdt; B. Pathiraj and B.H. Kolster, *Proceedings of the 2nd International Conference on Residual Stresses ICRS 2*, Elsevier Applied Science, 216 (1989).

10. P.C. Brand and H.J. Prask, *J. Appl. Cryst*, **27**, 164-176 (1994).

11. H.J. Prask, R.J. Fields, P.C. Brand, J.M. Blackburn, *Proceedings of the 4th International Conference on Residual Stresses, ICRS4*, Society for Experimental Mechanics, Inc., pp1198-1204 (1994).

12. P.C. Brand; Th. H. de Keijser and G. den Ouden, *Welding Journal, Research Supplement* **72**, pp 93s-100s (1993).

13. K. Masubuchi, *Analysis of welded structures*, Pergamon international library: series on materials and technology; 33, Oxford 1980, pp191-193.

14

Table captions

Table 1. Set of welding parameters of the available specimens.
Table 2. Orientations at which the strain was measured during the neutron diffraction measurements.
Table 3. Residual stresses in specimen A1.
Table 4. Residual stresses in specimen C2.
Table 5. Residual stresses in specimen S1.
Table 6. Residual stresses in specimen T2.

Figure captions

Figure 1. Specified weld pattern and dimensions.
Figure 2. Examples of nonconforming welds
Figure 3. Schematic of the SMAW welding process.
Figure 4. Measurement geometry showing the weld end and the weld start around a "skip" and the axis system of diffraction residual stress measurements.
Figure 5. Overview of measurement sites for the neutron and x-ray diffraction stress measurements.
Figure 6. a) Specimen A1, σ_L
          b) Specimen A1, σ_T
          c) Specimen A1, τ_{TL}
          d) Specimen A1, σ_Z
Figure 7. a) Specimen C2, σ_L
          b) Specimen C2, σ_T
          c) Specimen C2, τ_{TL}
          d) Specimen C2, σ_Z
Figure 8. a) Specimen S1, σ_L
          b) Specimen S1, σ_T
          c) Specimen S1, τ_{TL}
          d) Specimen S1, σ_Z
Figure 9. a) Specimen T2, σ_L
          b) Specimen T2, σ_T
          c) Specimen T2, τ_{TL}
          d) Specimen T2, σ_Z

Table 1

Set of welding parameters of the available specimens.
General parameters are:

Base Material: A515-70 steel
Sizes: 61 cm × 15 cm (24" × 6") and
                        61 cm x 13 cm (24" × 5")
Electrode: 5 mm (3/16") diameter E7018
Weld Type: One path skip bead-on-plate welds
Welding Method: Shielded metal arc Welding (SMAW)

Specimen ID	Welding Current	Travel Speed		Leading Angle
	(A)	(cm/min)	(inch/min)	(Degrees)
S1	230	10	4	20
S2	230	10	4	20
A1	230	10	4	0
A2	230	10	4	45
C1	200	10	4	20
C2	270	10	4	20
T1	230	7.5	3	20
T2	230	15	6	20

Table 2

Orientations at which the strain was measured during the neutron diffraction measurements.

φ	ψ	Remarks
0°	0°	Neutron beam in and out on same plate surface
90°	0°	Neutron beam in and out on opposite plate surfaces
90°	30°	
90°	60°	
90°	90°	

17

Neutron Measurements taken 9 mm below the welded surface — A1

Distance from WCL	Distance from weld end			Distance to weld start		
	1.5 mm	4.5 mm	7.5 mm	7.5 mm	4.5 mm	1.5 mm
-11 mm	36	← σ_L				8
	-98	← σ_T				-114
	99	← τ_{LT}				120
	-71	← σ_Z				-111
-6 mm	72					17
	-105	Neutron Measurements taken				-112
	61	9 mm below the welded surface				46
	-51	A1				-66
-3 mm	-8					12
	-140					-164
	34					30
	-129					-85
0 mm	69	59	48	66	78	63
	-91	-142	-164	-146	-151	-139
	-12	4	-2	-8	37	17
	-75	-56	-13	-5	-40	-51
3 mm	12					17
	-118					-138
	-41					-23
	-99					-104
6 mm	64					57
	-97					-100
	-87					-10
	-102					-81
11 mm	11					-14
	-56					-141
	-114					-93
	-65					-97

Neutron Measurements taken 6 mm below the welded surface — A1

Distance from WCL	Distance from weld end			Distance to weld start		
	1.5 mm	4.5 mm	7.5 mm	7.5 mm	4.5 mm	1.5 mm
-11 mm	36	← σ_L				40
	-81	← σ_T				-75
	79	← τ_{LT}				85
	-45	← σ_Z				-10
6 mm	16					64
	-144	Neutron Measurements taken				-85
	75	6 mm below the welded surface				91
	-123	A1				-72
-3 mm	77					70
	-130					-91
	7					40
	-118					-14
0 mm	13	48	29	57	62	52
	-206	-132	-156	-135	-115	-131
	33	10	3	-8	17	-2
	-143	-43	-41	0	-41	-39
3 mm	16					61
	-135					-141
	-33					-41
	-124					-56
6 mm	53					31
	-70					-99
	-75					-51
	-90					-36
11 mm	-16					16
	-112					-106
	-74					-99
	-113					-61

Neutron Measurements taken 3 mm below the welded surface — A1

Distance from WCL	Distance from weld end			Distance to weld start		
	1.5 mm	4.5 mm	7.5 mm	7.5 mm	4.5 mm	1.5 mm
-11 mm	70	← σ_L				76
	-138	← σ_T				-66
	71	← τ_{LT}				122
	-67	← σ_Z				-16
-6 mm	23					70
	-181	Neutron Measurements taken				-107
	48	3 mm below the welded surface				80
	-126	A1				-97
-3 mm	148					126
	-112					-81
	11					68
	-60					-83
0 mm	144	68	102	44	68	130
	-128	-122	-131	-139	-129	-112
	20	19	-12	-1	-1	-14
	-51	-24	-3	8	-4	-51
3 mm	180					52
	-67					-146
	-50					-59
	9					-133
6 mm	66					104
	-135					-72
	-34					-40
	-80					-59
11 mm	81					81
	-101					-79
	-81					-100
	-56					-40

Table 3

Specimen A1
Current 230 A
Travel Speed 10 cm/min (4 ipm)
Leading Angle 0°

Stress values in MPa

X-ray Measurements taken 0.25 mm below the welded surface — A1

Distance from WCL	Distance from weld end			Distance to weld start		
	1.5 mm	4.5 mm	7.5 mm	7.5 mm	4.5 mm	1.5 mm
-6 mm	73	← σ_L				80
	-73	← σ_T				-57
	17	← τ_{LT}				86
0 mm	124					217
	-83	X-ray Measurements taken				-62
	-3	0.25 mm below the welded surface				25
6 mm	93					100
	-83	A1				-16
	-35					-17

18

Distance from WCL	Distance from weld end			Distance to weld start		
	1.5 mm	4.5 mm	7.5 mm	7.5 mm	4.5 mm	1.5 mm
-11 mm	33	← σ_L				-23
	-83	← σ_T				-50
	93	← τ_{LT}				53
	-65	← σ_z				29
-6 mm	-18	Neutron Measurements taken				14
	-139	9 mm below the welded surface				-109
	59					75
	-133	C2				37
-3 mm	14					22
	-174					-112
	55					91
	-134					35
0 mm	13	32	35	-2	28	24
	-128	-134	-165	-204	-177	-117
	-14	-5	-27	19	13	52
	-133	-88	-62	-17	-74	36
3 mm	15					33
	-134					-113
	-58					37
	-114					31
6 mm	-47					74
	-119					-108
	-49					22
	-141					13
11 mm	9					35
	-74					-117
	-104					-68
	-109					32

Distance from WCL	Distance from weld end			Distance to weld start		
	1.5 mm	4.5 mm	7.5 mm	7.5 mm	4.5 mm	1.5 mm
-11 mm	3	← σ_L				3
	-88	← σ_T				-91
	82	← τ_{LT}				109
	-100	← σ_z				34
-6 mm	62	Neutron Measurements taken				24
	-73	6 mm below the welded surface				-79
	37					104
	-92	C2				21
-3 mm	-22					41
	-223					-78
	59					106
	-188					15
0 mm	80	26	-11	-1	57	41
	-127	-141	-151	-195	-160	-95
	-14	3	-13	-13	-2	87
	-136	-53	-87	-1	0	21
3 mm	43					29
	-102					-128
	-28					25
	-107					38
6 mm	69					42
	-56					-157
	-81					-28
	-73					45
11 mm	24					37
	-78					-123
	-69					-48
	-73					34

Distance from WCL	Distance from weld end			Distance to weld start		
	1.5 mm	4.5 mm	7.5 mm	7.5 mm	4.5 mm	1.5 mm
-11 mm	44	← σ_L				27
	-112	← σ_T				-104
	94	← τ_{LT}				146
	-93	← σ_z				30
-6 mm	63	Neutron Measurements taken				40
	-127	3 mm below the welded surface				-97
	66					114
	-96	C2				22
-3 mm	156					51
	-75					-96
	11					95
	-36					18
0 mm	158	57	43	15	43	98
	-47	-118	-146	-191	-131	-76
	-7	-41	-31	-12	-8	108
	-13	-78	-27	-27	-5	-9
3 mm	129					103
	-76					-108
	4					39
	-4					2
6 mm	86					134
	-84					-121
	-65					-17
	-47					-5
11 mm	69					104
	-66					-92
	-88					-64
	-60					-5

Table 4

Specimen C2
Current 270 A
Travel Speed 10 cm/min (4 ipm)
Leading Angle 20°

Stress values in MPa

Distance from WCL	Distance from weld end			Distance to weld start		
	1.5 mm	4.5 mm	7.5 mm	7.5 mm	4.5 mm	1.5 mm
-6 mm	72	← σ_L				77
	-112	← σ_T				-117
	43	← τ_{LT}				91
0 mm	114	X-ray Measurements taken				92
	-149	0.25 mm below the welded				-150
	35	surface				8
6 mm	102	C2				45
	-92					-117
	-59					-31

Distance from WCL	Distance from weld end			Distance to weld start		
	1.5 mm	4.5 mm	7.5 mm	7.5 mm	4.5 mm	1.5 mm
-11 mm	27 ← σ_L					-16
	-107 ← σ_T					-78
	132 ← τ_{LT}					40
	-115 ← σ_Z					-69
-6 mm	82	Neutron Measurements taken				30
	-104	9 mm below the welded surface				-113
	70					73
	-89	S1				-23
-3 mm	124					-8
	-48					-185
	-7					66
	-44					-102
0 mm	79	72	17	37	61	36
	-94	-141	-193	-195	-151	-162
	-9	-11	-27	-10	-37	46
	-100	-49	-56	-14	-37	-65
3 mm	129					10
	-10					-183
	-89					20
	-36					-80
6 mm	57					32
	-52					-198
	-75					-8
	-59					-93
11 mm	11					9
	-100					-151
	-86					-81
	-69					-76

Distance from WCL	Distance form weld end			Distance to weld start		
	1.5 mm	4.5 mm	7.5 mm	7.5 mm	4.5 mm	1.5 mm
-11 mm	71 ← σ_L					11
	-96 ← σ_T					-95
	78 ← τ_{LT}					117
	-82 ← σ_Z					-34
-6 mm	88	Neutron Measurements taken				25
	-74	6 mm below the welded surface				-96
	50					106
	-54	S1				-24
-3 mm	109					57
	-115					-101
	13					90
	-41					-33
0 mm	96	59	64	65	57	28
	-121	-151	-164	-170	-146	-157
	-14	-17	-24	-30	-35	48
	-86	-30	-31	38	-2	-62
3 mm	86					44
	-101					-153
	-60					29
	-50					-42
6 mm	90					59
	-48					-174
	-99					-11
	-32					-38
11 mm	69					32
	-67					-132
	-87					-83
	-50					-74

Distance from WCL	Distance form weld end			Distance to weld start		
	1.5 mm	4.5 mm	7.5 mm	7.5 mm	4.5 mm	1.5 mm
-11 mm	111 ← σ_L					19
	-104 ← σ_T					-95
	77 ← τ_{LT}					136
	-26 ← σ_Z					-17
-6 mm	116	Neutron Measurements taken				65
	-107	3 mm below the welded surface				-79
	52					109
	-34	S1				-13
-3 mm	134					72
	-109					-110
	28					101
	-88					-74
0 mm	150	75	65	42	75	56
	-121	-138	-170	-156	-157	-151
	-10	-5	4	-33	-28	62
	-65	-26	2	-35	7	-107
3 mm	103					154
	-116					-107
	-35					19
	-75					-58
6 mm	95					98
	-97					-147
	-78					-51
	-46					-107
11 mm	85					55
	-98					-83
	-83					-104
	-22					-62

Table 5

Specimen S1
Current 230 A
Travel Speed 10 cm/min (4 ipm)
Leading Angle 20°

Stress values in MPa

Distance from WCL	Distance form weld end			Distance to weld start		
	1.5 mm	4.5 mm	7.5 mm	7.5 mm	4.5 mm	1.5 mm
-6 mm	-37 ← σ_L					89
	-157 ← σ_T					-74
	58 ← τ_{LT}					21
0 mm	-114	X-ray Measurements taken				189
	-241	0.25 mm below the welded				-53
	36	surface				-23
6 mm	-55					96
	-145	S1				-72
	-26					-77

Distance from WCL	Distance from weld end			Distance to weld start		
	1.5 mm	4.5 mm	7.5 mm	7.5 mm	4.5 mm	1.5 mm
-11 mm	41	$\leftarrow \sigma_L$				27
	-120	$\leftarrow \sigma_T$				-63
	86	$\leftarrow \tau_{LT}$				67
	-59	$\leftarrow \sigma_Z$				-41
-6 mm	72	Neutron Measurements taken				54
	-130	9 mm below the welded surface				-101
	16					86
	-108	T2				-56
-3 mm	67					63
	-122					-136
	-20					56
	-84					-54
0 mm	73	51	71	52	173	72
	-60	-204	-233	-237	-129	-154
	-67	-31	-28	-2	2	13
	-79	-75	-52	-50	11	-65
3 mm	21					52
	-61					-159
	-70					-19
	-49					-118
6 mm	-51					50
	-74					-159
	-71					-62
	-110					-90
11 mm	-63					20
	-48					-99
	-40					-56
	-92					-89

Distance from WCL	Distance from weld end			Distance to weld start		
	1.5 mm	4.5 mm	7.5 mm	7.5 mm	4.5 mm	1.5 mm
-11 mm	83	$\leftarrow \sigma_L$				46
	-111	$\leftarrow \sigma_T$				-84
	88	$\leftarrow \tau_{LT}$				114
	-29	$\leftarrow \sigma_Z$				-39
-6 mm	95	Neutron Measurements taken				100
	-141	6 mm below the welded surface				-98
	12					111
	-52	T2				-20
-3 mm	66					88
	-169					-137
	-18					71
	-76					-58
0 mm	108	95	85	110	117	82
	-102	-168	-203	-154	-169	-199
	-96	-35	-11	-5	-15	17
	-26	-19	-38	18	-22	-74
3 mm	90					110
	-67					-157
	-129					-5
	-33					-56
6 mm	61					56
	-104					-160
	-121					-75
	-83					-84
11 mm	-34					12
	-101					-128
	-70					-116
	-62					-50

Distance from WCL	Distance from weld end			Distance to weld start		
	1.5 mm	4.5 mm	7.5 mm	7.5 mm	4.5 mm	1.5 mm
-11 mm	158	$\leftarrow \sigma_L$				48
	-87	$\leftarrow \sigma_T$				-136
	65	$\leftarrow \tau_{LT}$				139
	-1	$\leftarrow \sigma_Z$				-61
-6 mm	215	Neutron Measurements taken				75
	-119	3 mm below the welded surface				-139
	20					87·
	-2	T2				-83
-3 mm	196					160
	-120					-85
	-44					59
	-21					-39
0 mm	97	130	91	54	116	201
	-139	-54	-92	-127	-98	-84
	-71	-30	-13	8	-34	16
	-76	-9	-33	-39	-17	-47
3 mm	104					157
	-154					-146
	-106					-40
	-39					-113
6 mm	78					127
	-160					-102
	-99					-78
	-45					-57
11 mm	-8					80
	-122					-114
	-108					-139
	-55					-36

Table 6

Specimen T2
Current 230 A
Travel Speed 15 cm/min (6 ipm)
Leading Angle 20°

Stress values in MPa

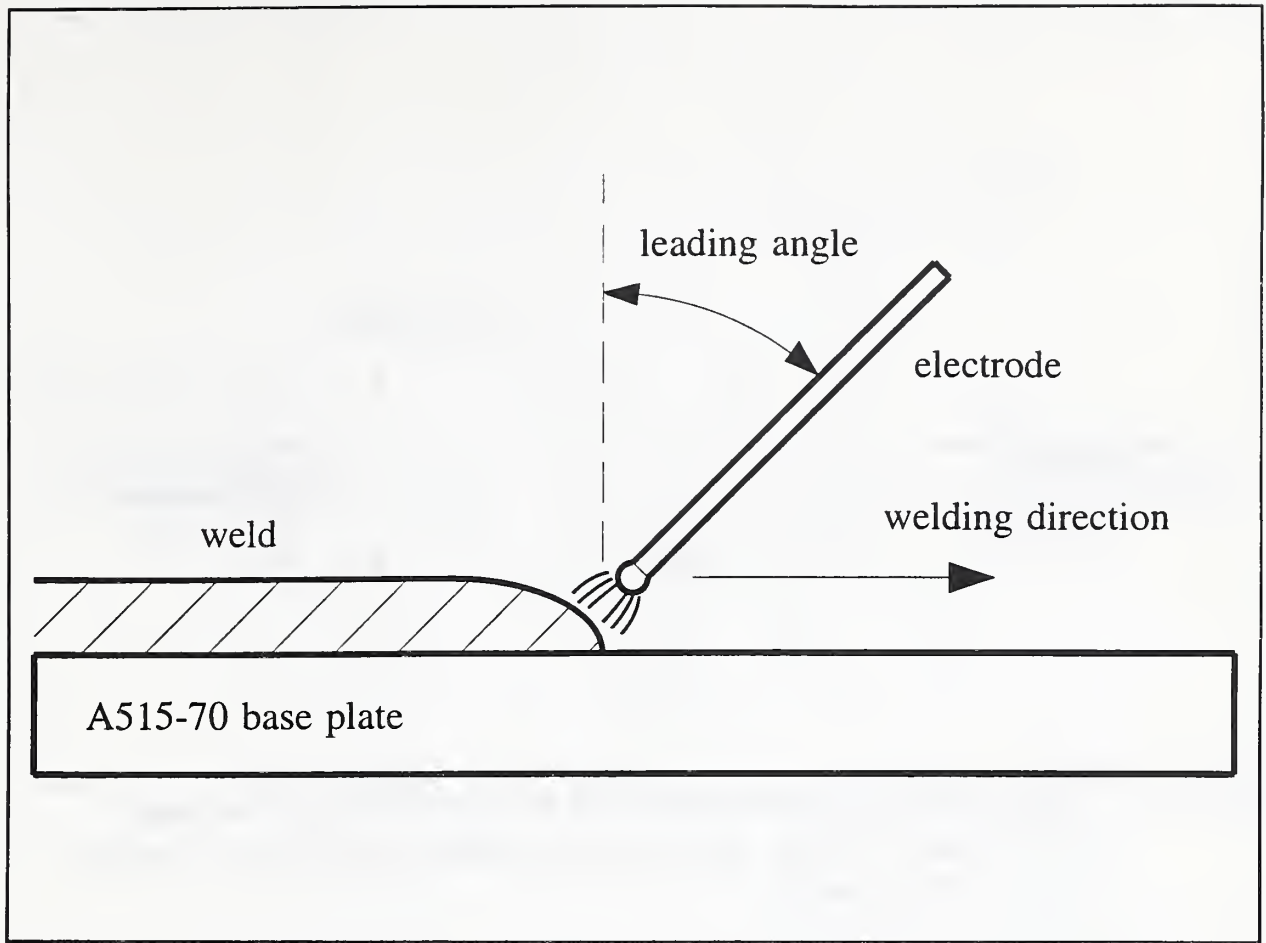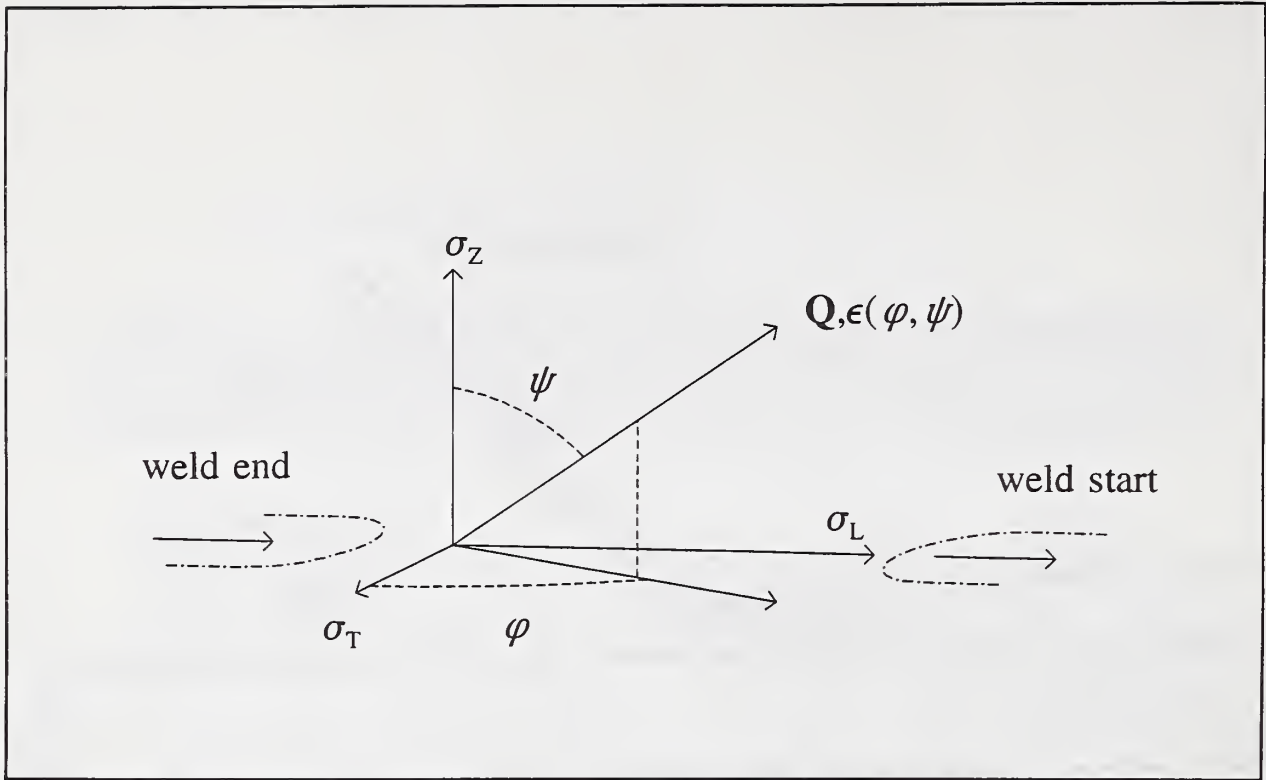| Distance from WCL	Distance from weld end			Distance to weld start		
	1.5 mm	4.5 mm	7.5 mm	7.5 mm	4.5 mm	1.5 mm
-6 mm	31	$\leftarrow \sigma_L$				76
	-102	$\leftarrow \sigma_T$				-2
	21	$\leftarrow \tau_{LT}$				58
0 mm	65	X-ray Measurements taken				140
	-139	0.25 mm below the welded				-51
	20	surface				15
6 mm	0					90
	-107	T2				-33
	-42					-75

21

Figure 1 Specified weld pattern and dimensions.
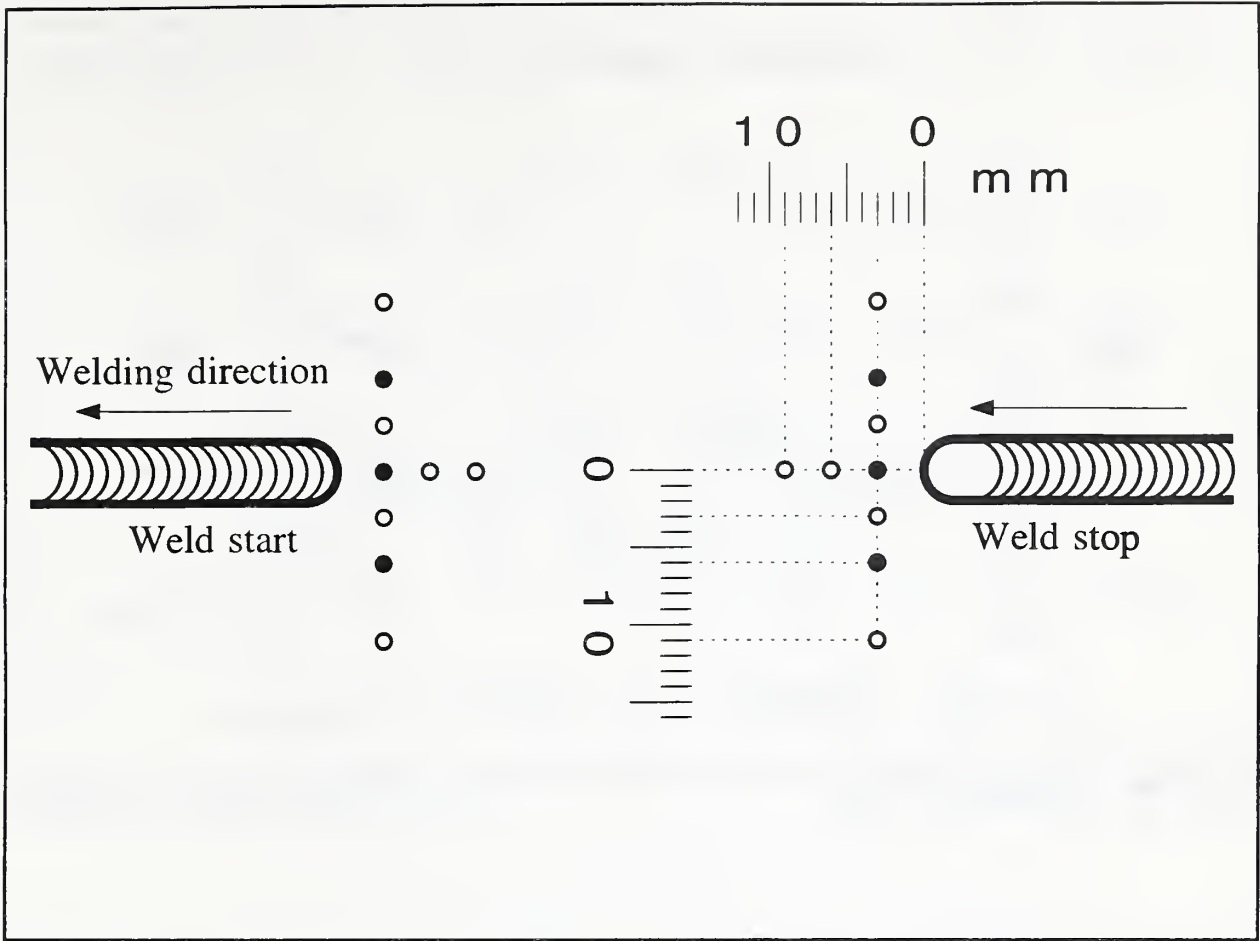
Figure 2 Examples of nonconforming welds.

Figure 3   Schematic of the SMAW welding process.

Figure 4   Measurement geometry showing the weld end and the weld start around a "skip" and the axis system of diffraction residual stress measurements.

Figure 5   Overview of measurement sites for the neutron and x-ray diffraction stress measurements. The closed symbols represent the X-ray surface measurement sites. Sub-surface neutron residual stress measurements were performed at both open and closed symbol positions (at three different depths below the surface *viz.* 3, 6 and 9 mm below the surface).
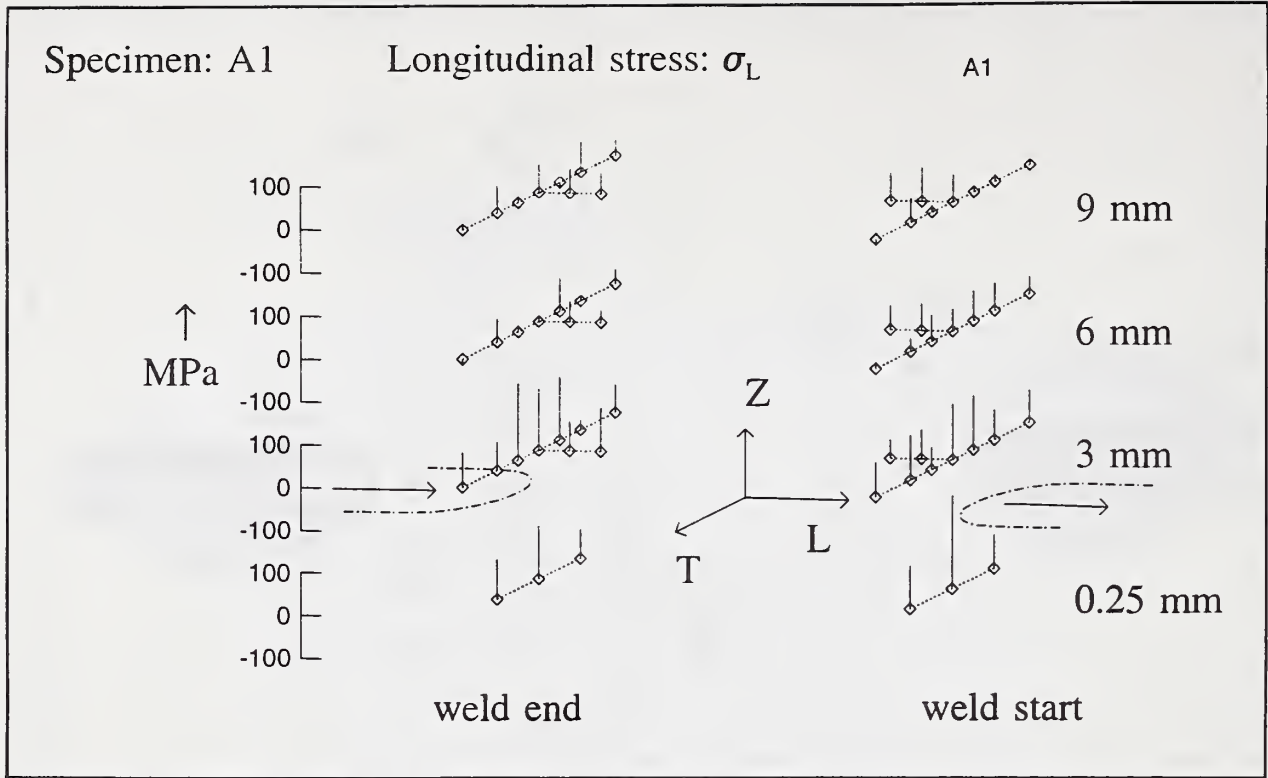
Figure 6a Specimen A1, σ_L
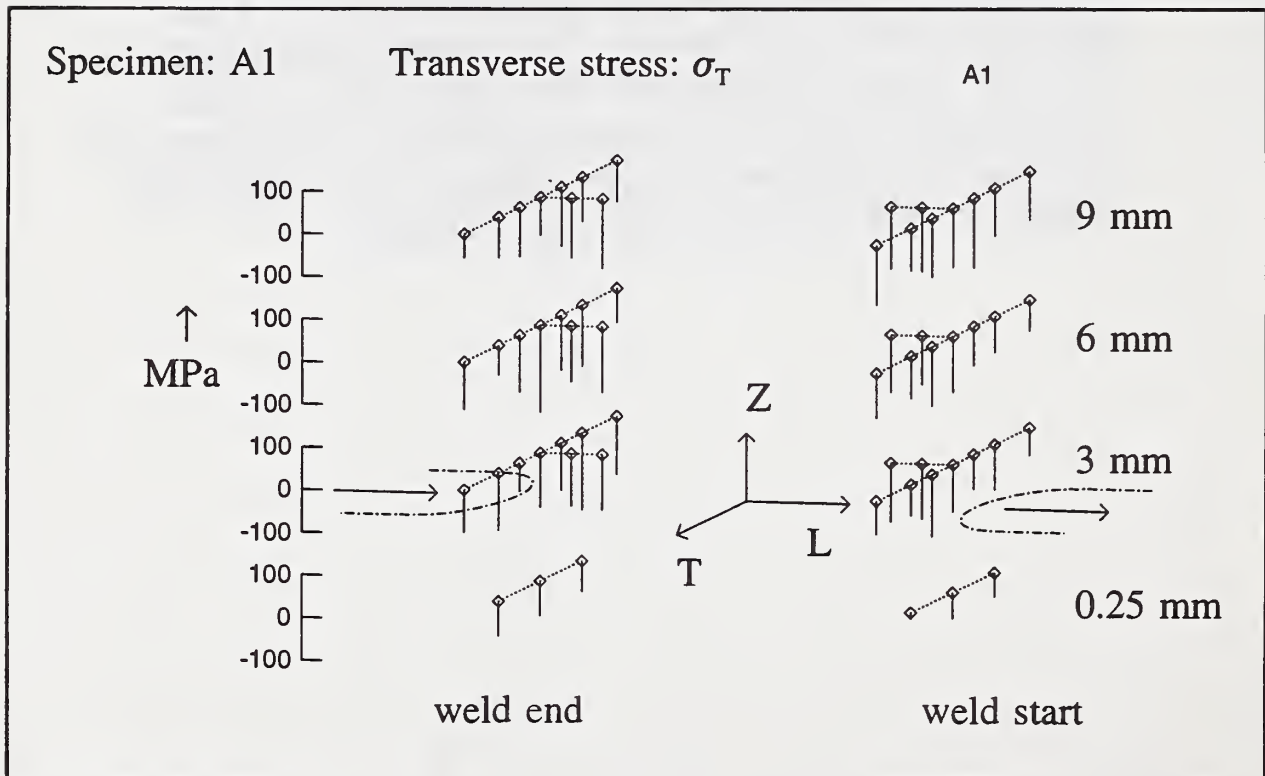
Figure 6b Specimen A1, σ_T

28
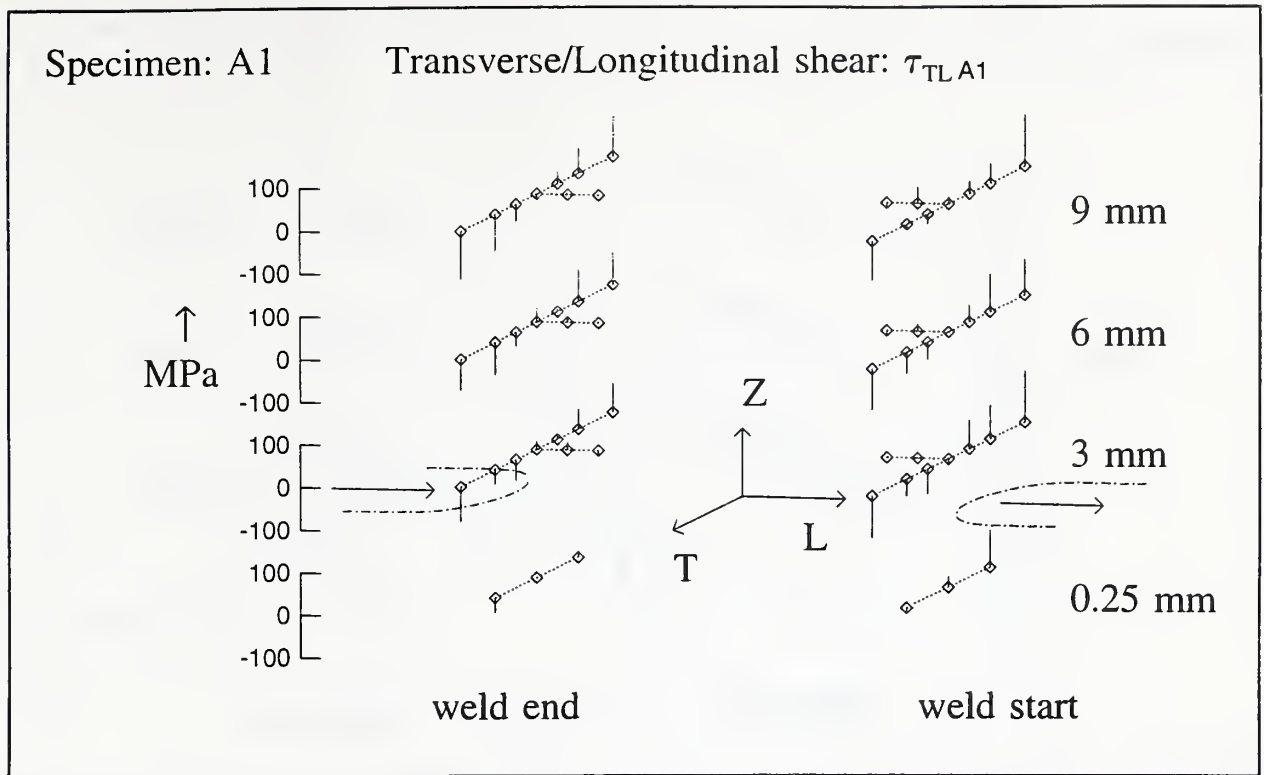
Figure 6c Specimen A1, τ_{TL}
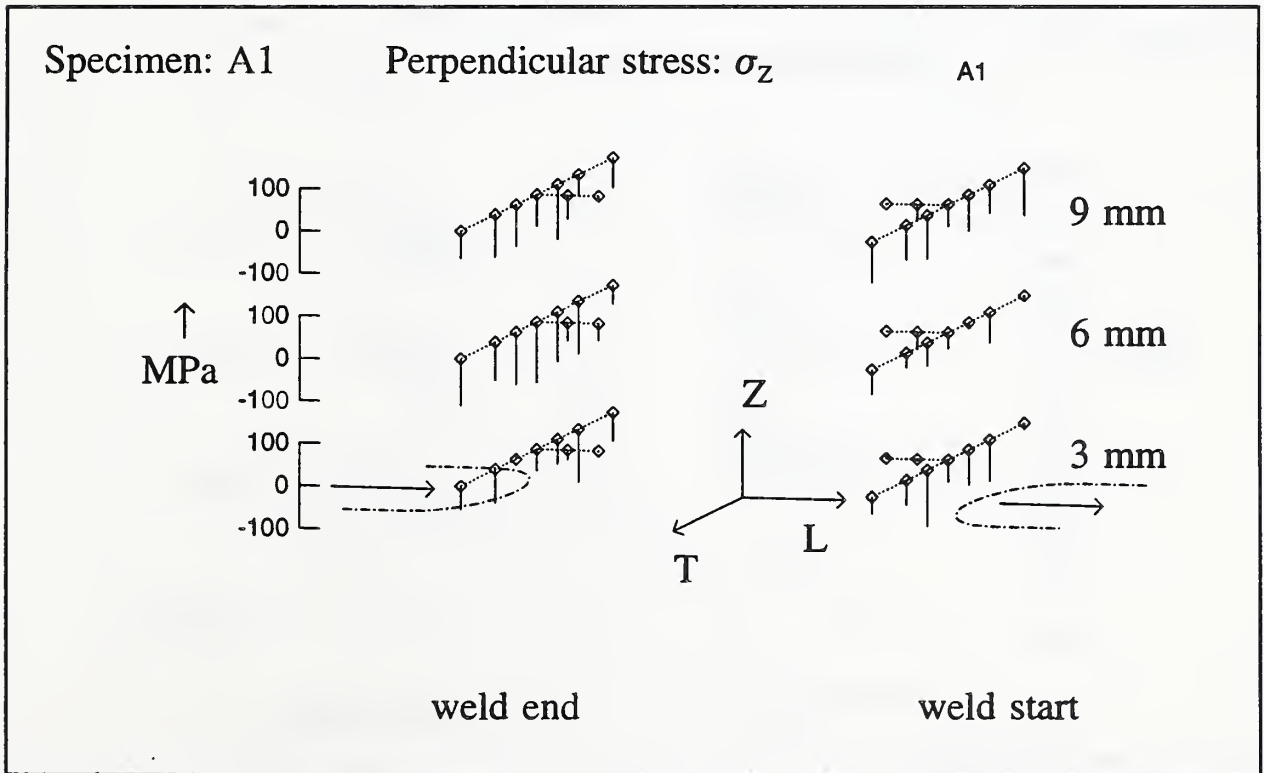
Figure 6d Specimen A1, σ_Z

29
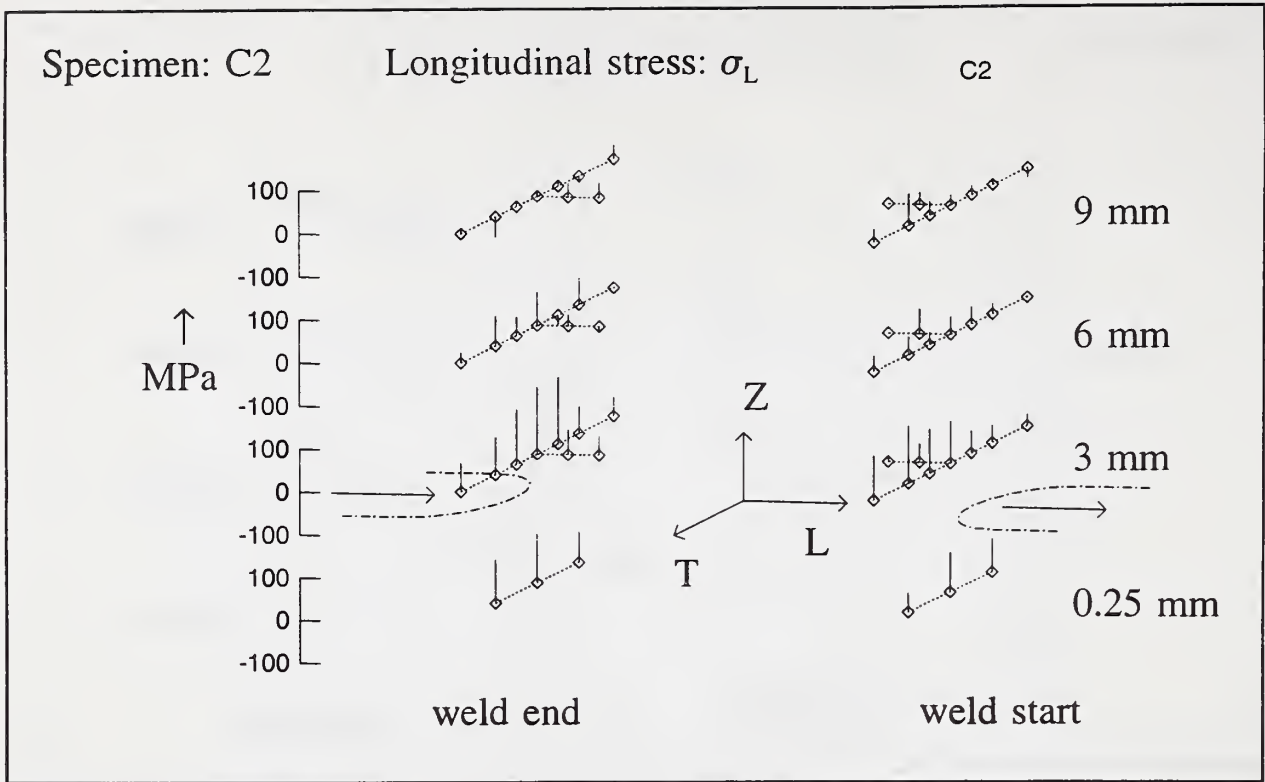
Figure 7a Specimen C2, σ_L
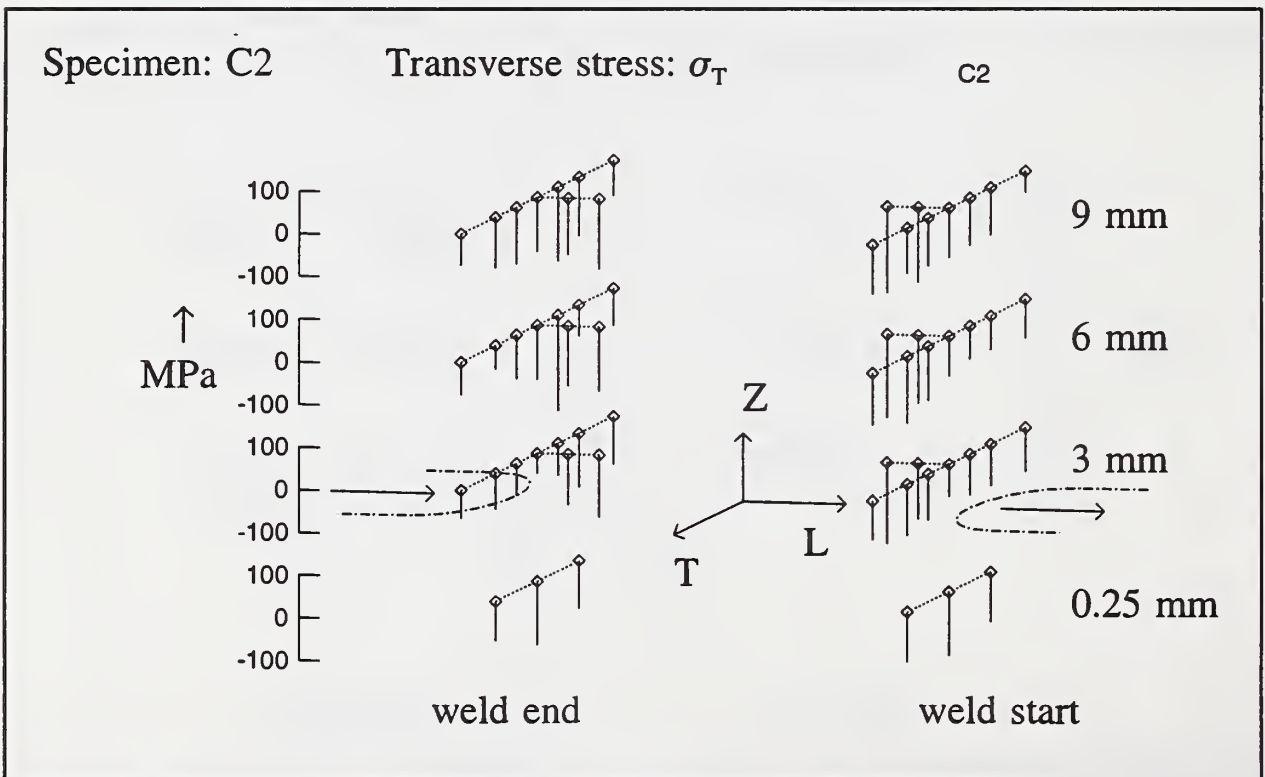
Figure 7b Specimen C2, σ_T
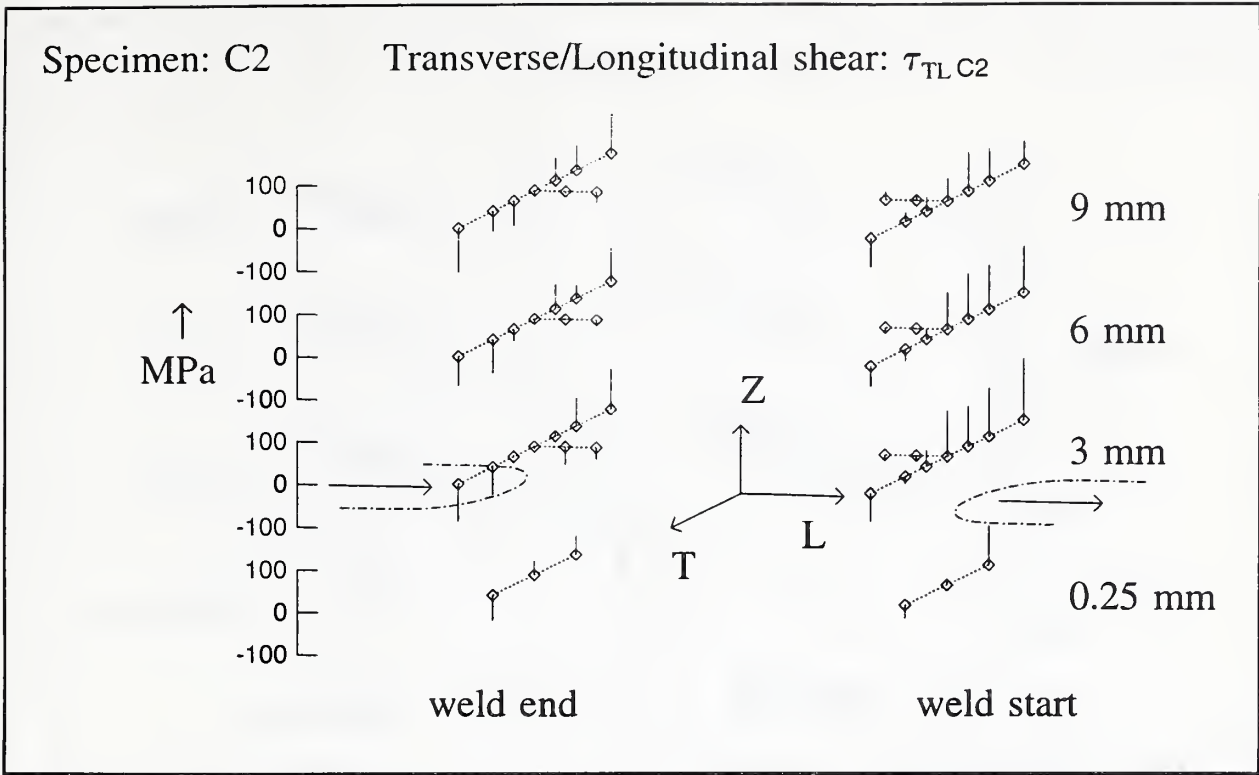
Figure 7c Specimen C2, τ_{TL}
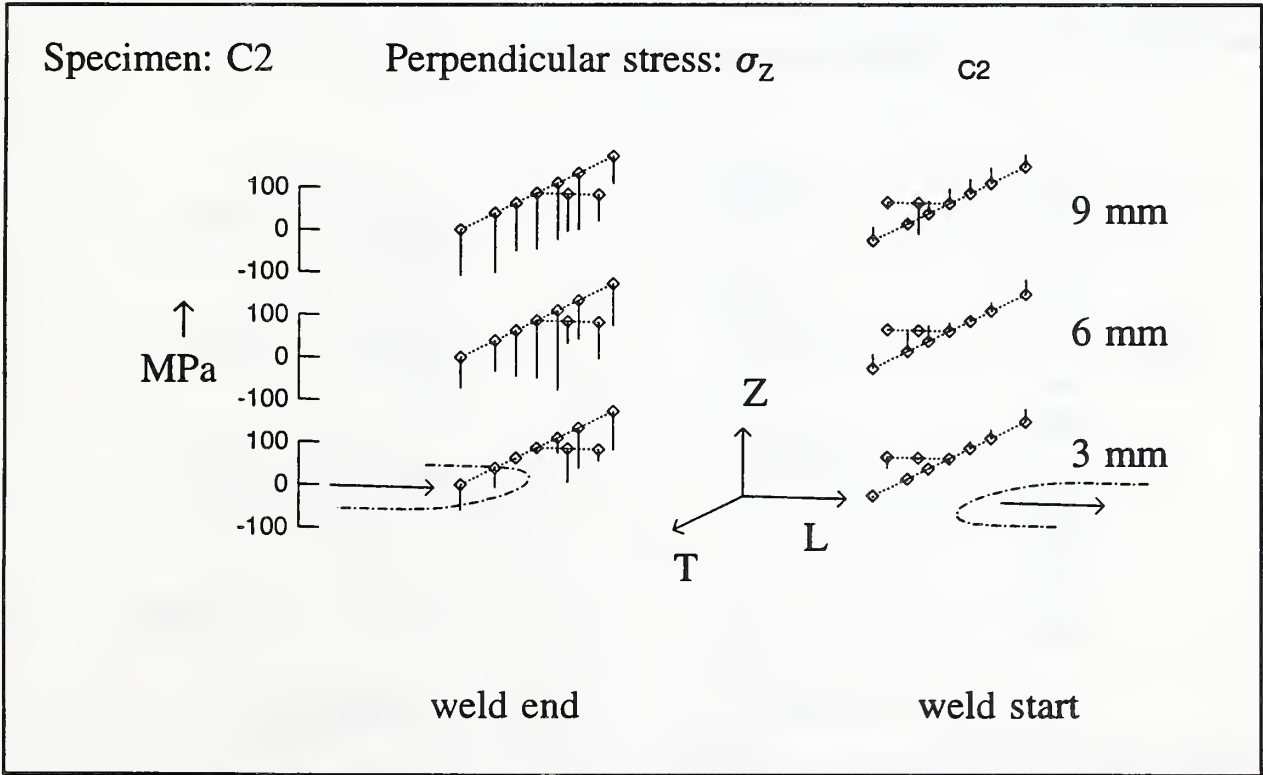
Figure 7d Specimen C2, σ_Z

31
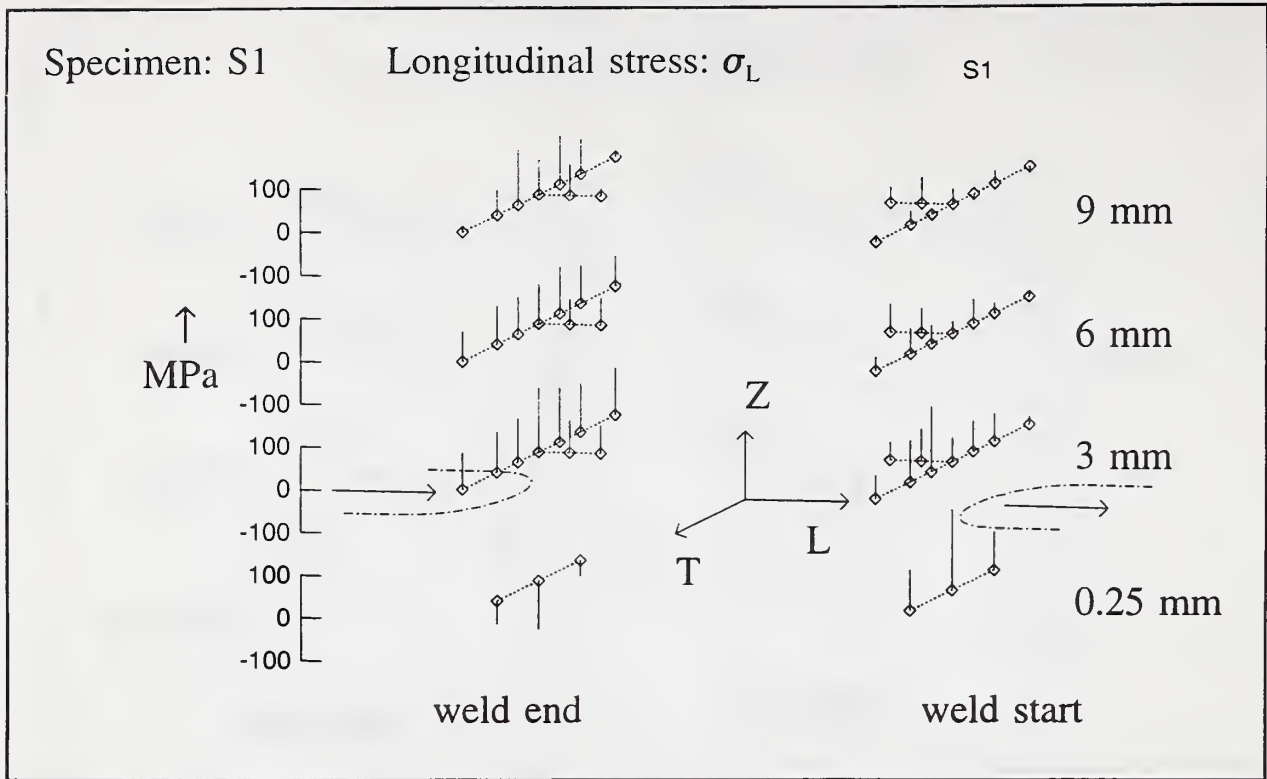
Figure 8a Specimen S1, σ_L
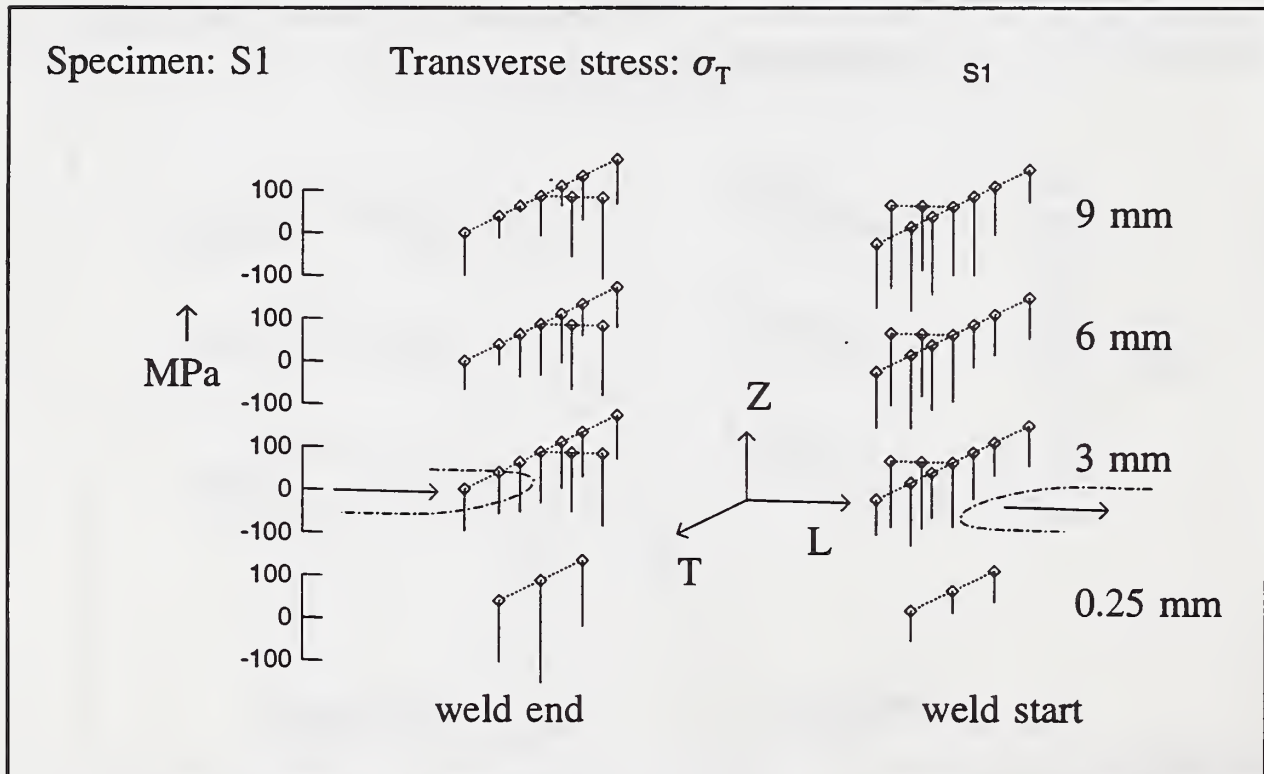
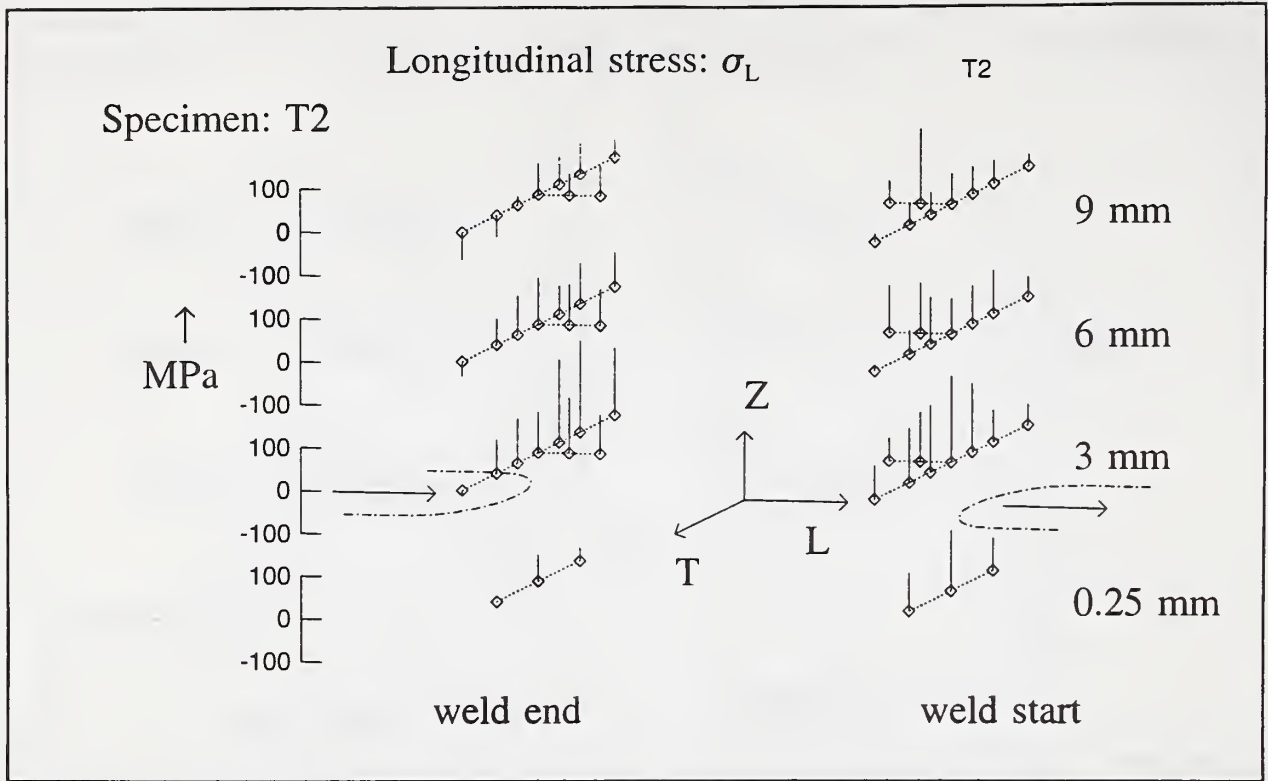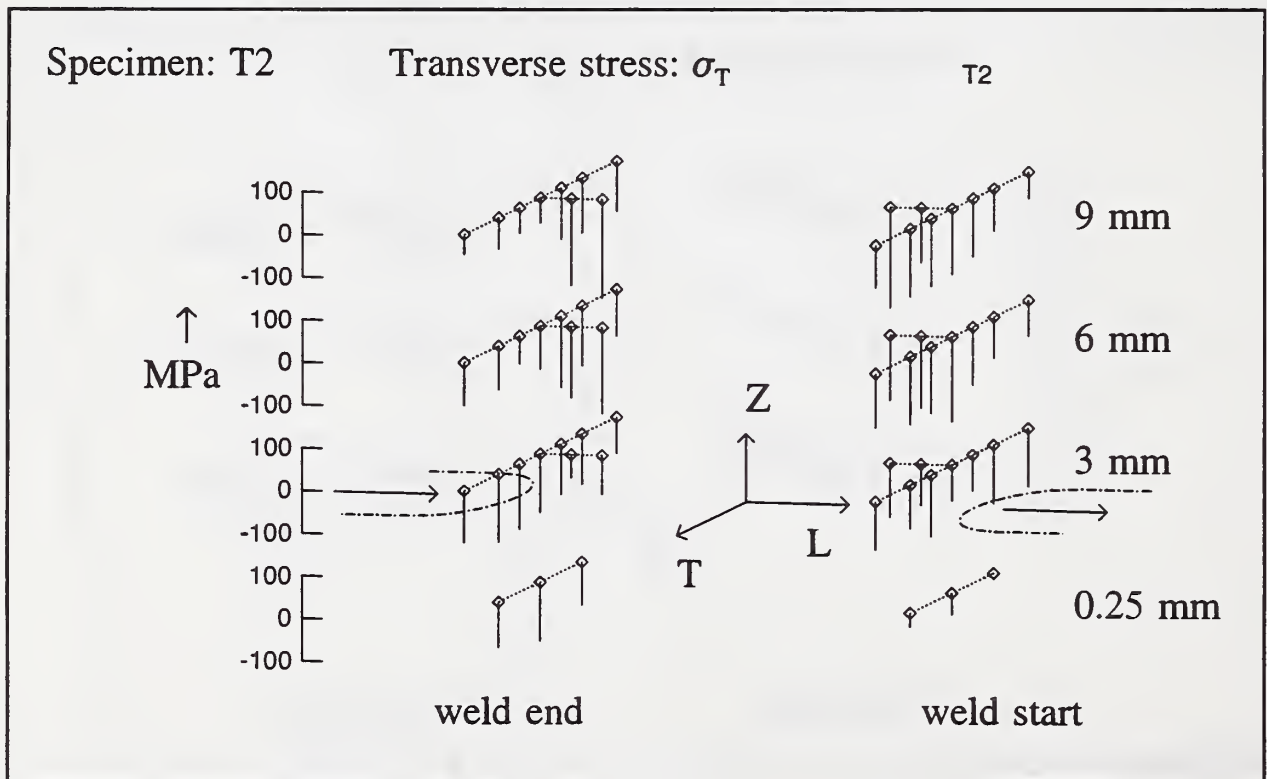**Figure 8b** Specimen S1, σ_T
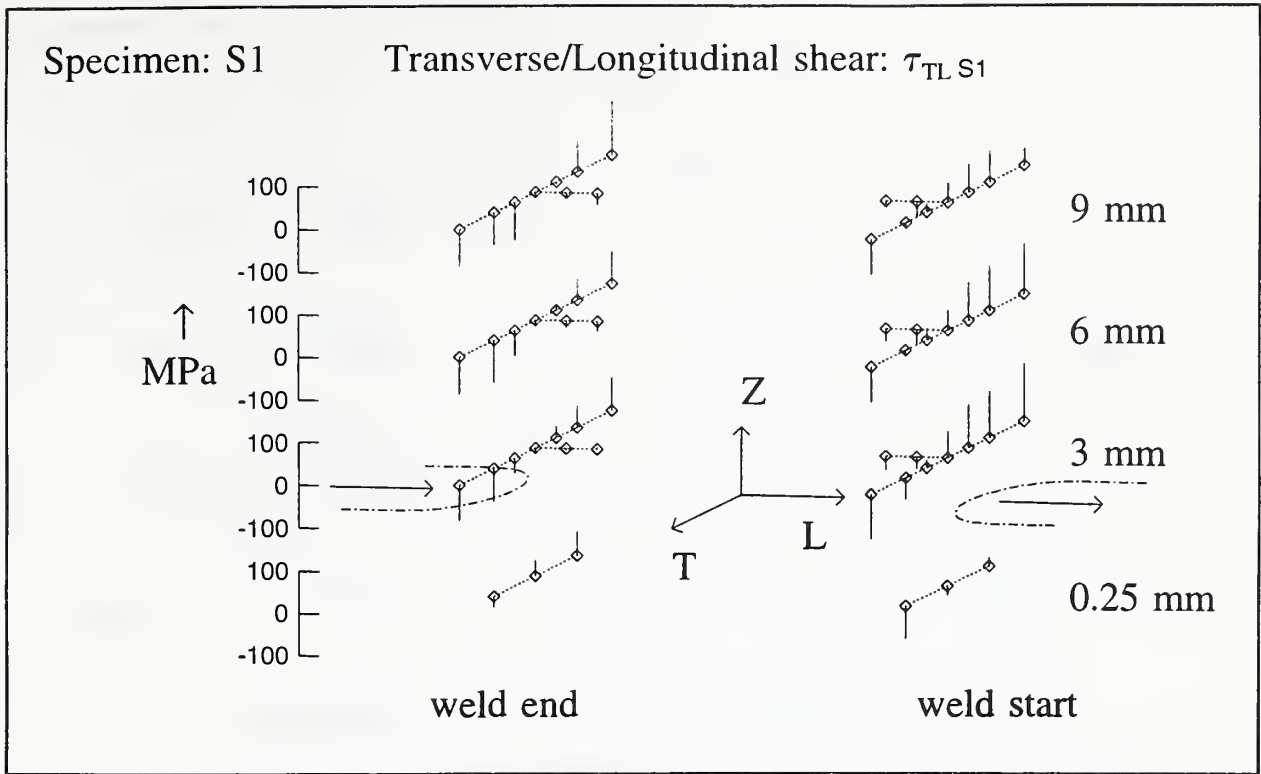
Figure 8c Specimen S1, τ_{TL}
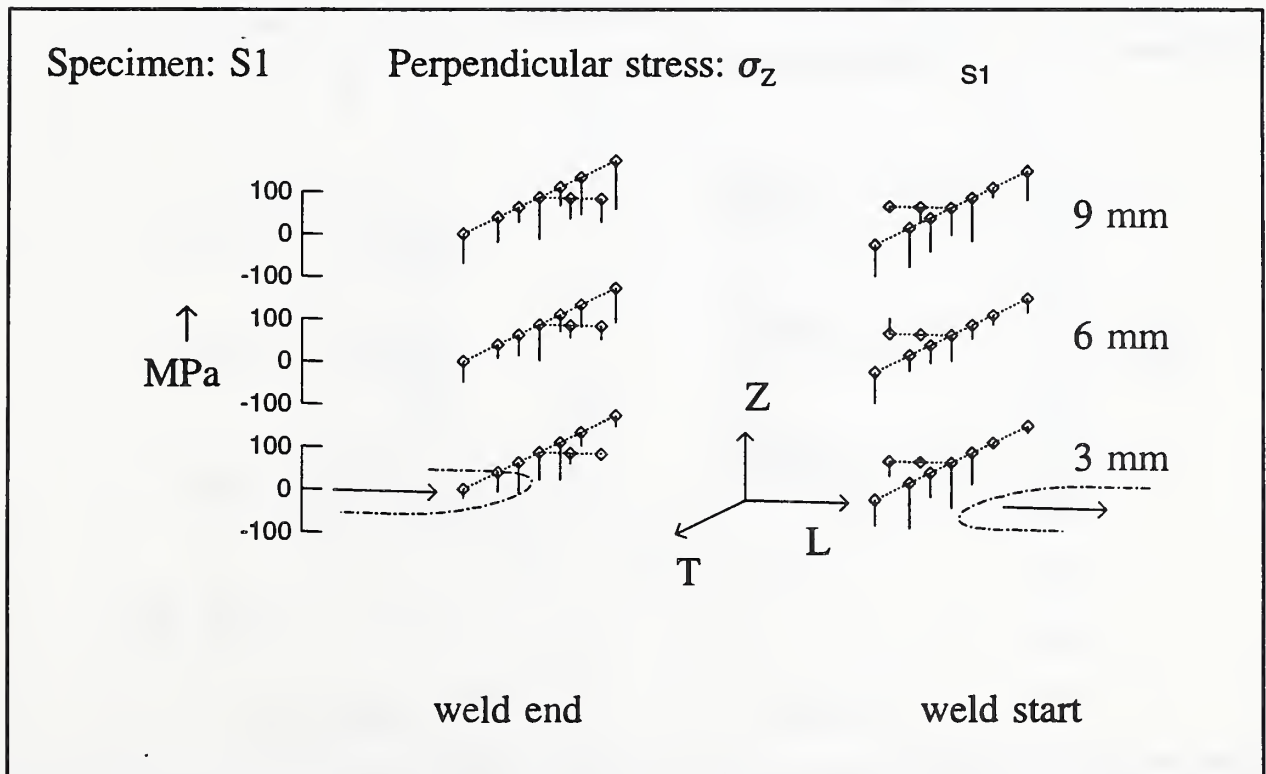
Figure 8d Specimen S1, σ_Z

33

Figure 9a Specimen T2, σ_L
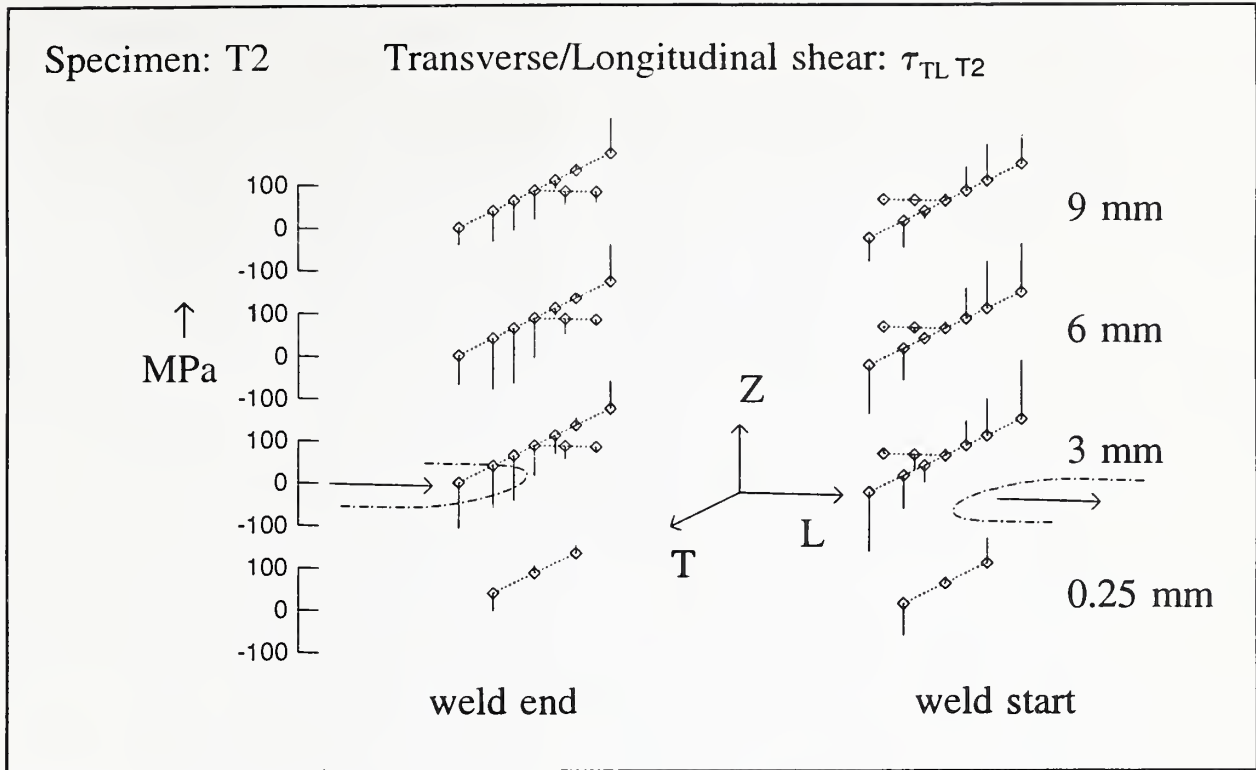

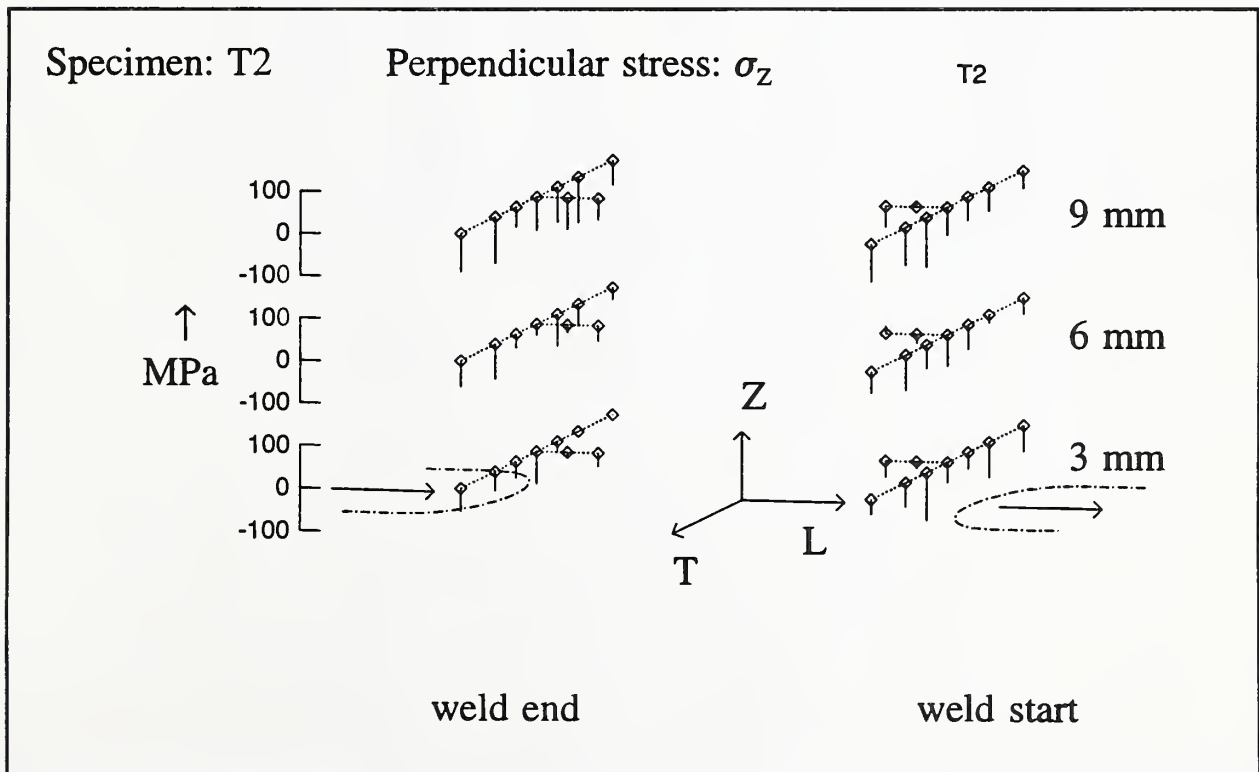**Figure 9b** Specimen T2, σ_T

Figure 9c Specimen T2, τ_{TL}

Figure 9d Specimen T2, σ_Z

35